Single-mode optically activated phase modulator on GaAs/GaAlAs compound semiconductor rib waveguides

R. T. Chen
Microelectronics Research Center, Department of Electrical and Computer Engineering, University of Texas, Austin, Austin, Texas 78712

R. Shih, D. Robinson, and T. Jannson
Physical Optics Corporation, 2545 West 237th Street, Torrance, California 90505

(Received 23 March 1992; accepted for publication 5 August 1993)

We report on an optically activated phase modulator (OAM) and modulator array on GaAs-GaAlAs compound semiconductor rib waveguides. A rib waveguide device with an optical activation window of 5 μm in diameter was fabricated. Optical activation was produced by using a HeNe 632.8 nm wavelength as the free-carrier generator and a 1.3 μm laser as the signal carrier. A 33% modulation depth was observed and 10^{-2} index modulation was experimentally confirmed on an OAM working in the phase modulation regime. OAMs working in both phase- and cutoff-modulation regimes were further determined by considering the variation of the waveguide confinement factor. An 8.2 dB modulation depth was observed on an OAM working at the cutoff regime. Furthermore, the activation source for the free-carrier generation is in the mW power region, which significantly reduces the size and cost of all optical switching devices.

I. INTRODUCTION

One of the major building blocks of an optoelectronic integrated circuit (OEIC) is the optically guided wave modulator. The realization of optical communication and computing with high parallelism, large modulation bandwidth, and low propagation loss have made the optical wave an attractive information carrier.

Within the past fifteen years, several types of guided wave electro-optic modulators have been built. The electro-optic modulation of light can be separated into phase,[1–5] polarization,[6,7] intensity,[8–10] and multiquantum well (MQW) modulation. The fundamental emphasis of electro-optic and all-optical modulators is focusing on changing the index of refraction of the optical and electro-optic materials within which the optical waves propagate. In this article, an optically activated modulator on a GaAs/GaAlAs compound semiconductor rib waveguide was successfully developed. The devices we report here can be used either as optically enhanced phase modulators or as optically activated cutoff modulators. The device parameters can be designed to satisfy the criterion needed for either case. The principle of operation and the device structure are introduced in Sec. II. Design rules for all-optical modulators are detailed as well.

Section II also includes a description of the fabrication procedure for the proposed device. The etching process, rib waveguide formation on the GaAs/GaAlAs substrate, optical window formation, rib waveguide edge cleavage to facilitate end-fire coupling, and device packaging are reported. Performance of the modulators and modulator arrays is detailed in Sec. III. Demonstration of optically activated phase modulators is presented first, followed by considerations for waveguide design, and reporting on optically activated modulators working at the cutoff boundary. The phase shift of the guided wave as a function of modulating optical wave (visible) is measured. Incorporation of a dc-biased voltage enhanced the modulation depth. The theoretically projected modulation speed is provided. The ultimate limitation on the speed of this type of device is the free-carrier lifetime of the semiconductor material involved. This is similar to counterpart microwave devices. For undoped GaAs the carrier lifetime is around 10 ns.[11] Carrier lifetime in the ps to sub-ps range has been achieved in GaAs by using doping or ion implantation techniques.[12,13] The results demonstrate that a device length even shorter than that for multiple quantum well devices is enough to provide a high extinction ratio for the optical throughput of the modulator. Depending on the application scenario, both all-optical and electro-optic modulators are realizable. Concluding remarks are made in Sec. IV.

II. PRINCIPLE OF OPERATION AND DEVICE STRUCTURE

GaAs provides a direct band gap, high electron and hole mobilities, and semi-insulating substrates. The combination of these characteristics allows us to make high speed, monolithic, optoelectronic integrated circuits. Optical waves with wavelengths within the 0.9–5 μm range can be used as the signal carrier. Optical photons from both coherent and incoherent light sources with $h\nu > E_g$ (i.e., the energy gap of GaAs waveguides) can be employed as the source for activating a vast number of free electrons and holes. The basic structure for the single-channel optically activated modulator (OAM) on a GaAs-GaAlAs waveguide is shown in Fig. 1. The small circular window area within the electrode pad is designed to input the optical photons with $h\nu > E_g$ to generate free electron and hole pairs. The optical wave representing the signal carrier can be coupled into the waveguide through end-firing or by

 0021-8979/93/74(10)/5964/8/$6.00

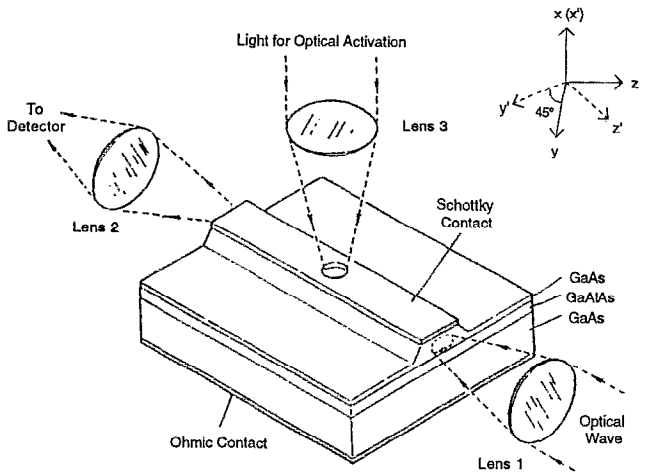

FIG. 1. Basic structure of optically activated modulator on GaAs.

a grating. A reverse bias (if needed) can be added across the Schottky barrier to form a depletion region to accelerate the free carriers.

A. The working principle

A discussion of the working principle of the modulator follows. A very large index change induced by current has been reported on Si,[14,15] GaAs-GaAlAs,[16–18] and InGaAsP-InP.[19,20] Since the current induced index change is much stronger than the linear electro-optic effect, an active device can be made by injecting a time dependent carrier concentration. The electron-hole pairs are first induced by shining strong condensed light, with photon energy larger than the band gap of the guiding layer material, on the window area shown in Fig. 1. A very large current density is induced in this way. When the optical signal carrier to be modulated is coupled to the ridge waveguide, the induced current will interact with the guided wave. It has been proven[14,15] that the change of index of refraction due to the injected free carriers can be two orders of magnitude higher than that generated by the linear electro-optic effect. A device interaction length compatible with multiquantum well structure is achievable using the proposed concept.

Another important factor is that in contrast to the linear electro-optic effect, which depends upon the vector electric field, the induced index change is a scalar function. If the effective masses of electrons and holes in the two different transverse directions are the same, then the induced change of the guiding layer index is the same for both TE and TM guided waves. This eases the requirement needed for the direction of waveguide propagation due to the isotropic characteristic.

As shown in Fig. 1, a Schottky contact is built on top of the rib waveguide. The reverse bias field added across the Schottky barrier is to increase photon generated electron-hole pairs (EHPs) within a diffusion length of the transition region in the semiconductor. The lack of free carriers within the space charge transition region can create a current due to the net generation of carriers by emission from recombination centers[21–23] and valence band to conduction band transition.

It is clear from the earlier discussion that an optically activated modulator does not depend on the orientation of the GaAs crystal. The free-carrier induced index modulation reduces the effective index of the guided mode isotropically. The device structure presented in Sec. II B allows experimental observation of the magnitude of the current-induced index modulation to be compared to the magnitude of the linear electro-optic effect.

To quantitatively compare the magnitude of the index modulation due to optical activation and to the linear electro-optic (EO) effect, an optical modulator that can work on both mechanisms needs to be built. For OAM, crystal orientation is not an influential factor. However, for GaAs, a cubic crystal that belongs to the symmetry group $\bar{4}3m$, the EO effect does depend on the orientation of the crystal. The EO tensor of GaAs may be written in the following form:

$$r_{ij}=\begin{pmatrix} 0 & 0 & 0 \\ 0 & 0 & 0 \\ 0 & 0 & 0 \\ r_{41} & 0 & 0 \\ 0 & r_{41} & 0 \\ 0 & 0 & r_{41} \end{pmatrix}. \tag{1}$$

The only nonvanishing elements are $r_{41}=r_{52}=r_{63}$. The index ellipsoid in the presence of a modulating electric field $\mathbf{E}(E_x,E_y,E_z)$ can be represented by the following quadratic equation:

$$\frac{x^2}{n_0^2}+\frac{y^2}{n_0^2}+\frac{z^2}{n_0^2}+2r_{41}E_xyz+2r_{41}E_yxz+2r_{41}E_zxy=1, \tag{2}$$

where the constants involved in the first three terms do not depend on the modulating field and, since the crystal is cubic, are designated as $n_x=n_y=n_z=n_0$. Thus, application of an electric field generates cross terms in the quadratic equation. For the device configuration shown in Fig. 1, since the electric field is applied along the x axis, Eq. (2) becomes

$$\frac{x^2+y^2+z^2}{n_0^2}+2r_{41}E_xyz=1. \tag{3}$$

The task at hand is to find a new coordinate system (x',y',z') in which the equation of the index ellipsoid, Eq. (2), contains no mixed terms; that is, it is of the form

$$\frac{x'^2}{n_{x'}^2}+\frac{y'^2}{n_{y'}^2}+\frac{z'^2}{n_{z'}^2}=1, \tag{4}$$

where x', y', and z' are then the major axes of the index ellipsoid in the presence of an external field applied along (100).

In the case of Eq. (3), it is clear that in order to eliminate the cross term we need to choose a coordinate system x',y',z', where x' is parallel to x. Because of the

symmetry of Eq. (3) in y and z, the coordinates y' and z' are related to y and z by a 45° rotation. The transformation relations from y,x to y',z' are thus

$$y=y'\cos 45°-z'\sin 45°, \tag{5}$$

$$z=y'\sin 45°+z'\cos 45°, \tag{6}$$

which, upon substitution in Eq. (3), yields

$$\left(\frac{1}{n_0^2}+r_{41}E_x\right)y'^2+\left(\frac{1}{n_0^2}-r_{41}E_x\right)z'^2+\frac{x^2}{n_0^2}=1. \tag{7}$$

This equation shows that x, y', and z' are indeed the principal axes of the index ellipsoid when a field is applied along the x direction. We also see that the length of the y' axis of the ellipsoid is $n_{y'}$, where

$$\frac{1}{n_{y'}^2}=\frac{1}{n_0^2}+r_{41}E_x. \tag{8}$$

Since in practice $r_{41}\ll n_0^2$, the following Taylor expansion is valid:

$$(1+r_{41}E_x n_0^2)^{-1/2}\approx 1-r_{41}E_x n_0^2/2. \tag{9}$$

Thus,

$$n_y'=n_0-n_0^3 r_{41}/2. \tag{10}$$

Similarly,

$$n_z'=n_0+n_0^3 r_{41}/2. \tag{11}$$

Finally,

$$n_x'=n_0. \tag{12}$$

Equation (7) shows that a rotation of 45° for the principal axes in the y-z plane results when an electric field is applied along the [100] direction in the basic modulator as shown in Fig. 1. It is to be noted that the ridge rib waveguide is oriented along the [011] on the (100) plane. We designed this structure to measure the magnitude of the index modulation due to generation of free carriers in comparison to modulation due to the well-known linear E-O effect. Note that the optically activated modulator working in both phase- and cutoff-modulation regimes can be realized on any orientation of GaAs crystal.

B. Device fabrication

A single-mode optically activated modulator and a linear array of identical modulators have been successfully fabricated. First, a planar GaAs-GaAlAs heterostructure with an aluminum concentration of approximately 7% was grown on an x-cut N^+ substrate using a metal-organic chemical-vapor deposition (MOCVD) system.[24] Planar waveguide formation was first confirmed experimentally through end-fire coupling. The rib waveguide and waveguide array were made through the conventional lithographic process. AZ1400 photoresist was employed as the masking material during the wet etching process which consisted of HCl, H_2O_2, and H_2O, in the ratio of 80:4:1, and provided an etching rate of 1.1 μm/min at room temperature. After the rib waveguide was empirically verified

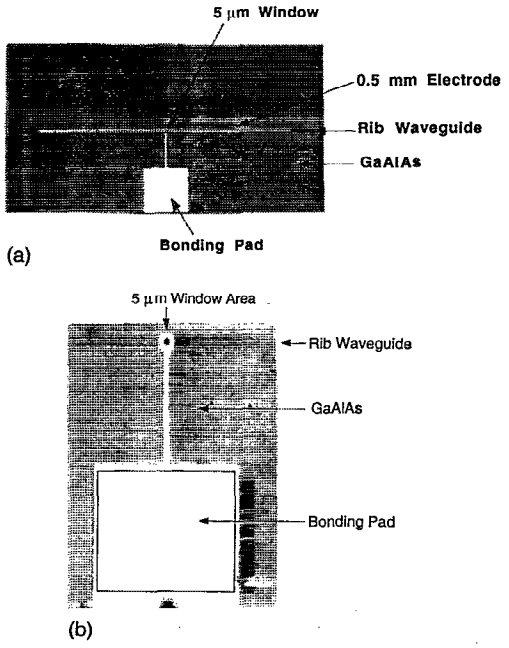

FIG. 2. (a) 0.5 mm electrode on a GaAs/GaAlAs rib waveguide and (b) 0.5- μm-diam window for optical activation on a single-mode GaAs/GaAlAs rib waveguide.

to be a successful optical guide, a thin Al film was deposited on the waveguide surface. A lift-off technique was employed to form the desired window for optical activation. A circular window 5 μm in diameter was formed on top of the rib waveguide. The microstructure revealed by a microscope is shown in Fig. 2(a). A key portion of the setup is detailed in Fig. 2(b), where the area of interaction is clearly indicated. The window area is located right on top of the GaAs rib waveguide within which the 1.3 μm laser light is propagating. The optical activation source can be introduced by using either an imaging lens (Fig. 1) or a single-mode fiber (not shown). The rib waveguide, Al electrode, and the 5-μm-diam window are clearly displayed.

TABLE I. Waveguide dimensions and orientations of GaAs/GaAlAs rib waveguide optically activated modulator and modulator array.

Common parameters	
Channel width	5 μm
Channel depth	1–1.5 μm
Waveguide type	Ridge channel
Etching solution	$HCl:H_2O_2:H_2O=80:4:1$
GaAlAs thickness	1 μm
Al concentration	7%
Schottky contact	Al 5000 Å thick
Substrate orientation	(100)
Waveguide direction	[011]
Window size (interaction length)	5 μm in diam
Cutoff modulator array	
Separation between adjacent channels	20 μm
Area of bonding pad	4 mil×4 mil
No. of channels	10
Packing density	500 channels/cm

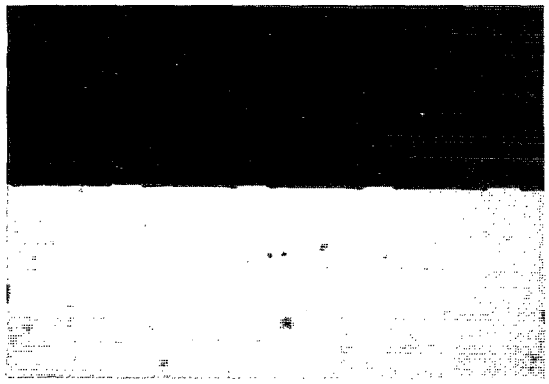

FIG. 3. Illustration of one of the cleaved end faces of the modulator array.

The parameters and waveguide orientations for both the basic modulator and the modulator array are given in Table I. Finally, after formation of an ohmic contact on the bottom face of the specimen, both end faces of the device were cleaved to facilitate edge coupling for subsequent experiments. Figure 3 shows a photograph of one of the cleaved end faces of the modulator array. The finished sample was then mounted on a special IC chip and placed in a device holder for detailed experimentation. The device package is shown in Fig. 4. Bonding wires, chip carrier, GaAs OAM, a 50 Ω microstrip line, and SMA connectors are clearly shown.

III. PERFORMANCE OF THE MODULATOR AND THE MODULATOR ARRAY

The experimental results are presented here. The setup employed to do the all-optical and the electro-optic measurement is described first. An optically activated modulator working in the phase modulator regime (well above the cutoff boundary) was produced. The feasibility of using the same device with a 0.5 mm electrode [Fig. 2(a)] as a linear electro-optic modulator is also introduced. Theoretical calculation was conducted using the confinement factor as an indicator to determine device criterion suitable for either the phase or cutoff regime. The result of the calculation is summarized in Sec. III C. Further results of the optically activated and electro-optic cutoff modulator are reported in Sec. III D.

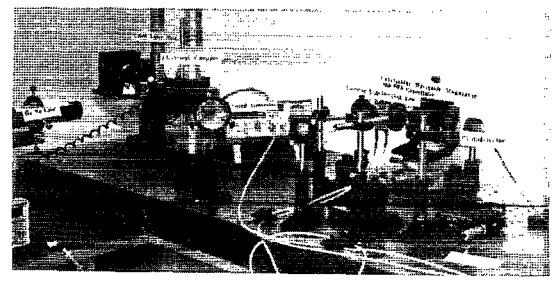

FIG. 5. Setup for OAM on a GaAs/GaAlAs rib waveguide.

A. Experimental setup

The setup employed for the demonstration is shown in Fig. 5, where the optical activation source (0.632 μm HeNe), 1.3 μm laser diode, GaAs/GaAlAs rib waveguide modulator package, coupling and imaging lenses, Ge photodetector (PIN), and the signal generator are clearly shown. The coupling lens provides a diffraction-limited beam waist at the input edge of the waveguide OAM. The imaging lens transfers the near field image of the throughput light from the rib waveguide to the detector. A near field image of the guided wave (1.3 μm) taken by a vidicon camera is illustrated in Fig. 6. The background noise was filtered out after the Fourier transform lens. Modulation of the device is observed through an oscilloscope.

B. Optically activated phase modulator

The first device we demonstrated was a single-mode optically activated phase modulator. By shining the HeNe 0.632 μm on the 5-μm-diam window area, we generated a 33% modulation depth in reference to Fig. 7. The results we demonstrated provide us with not only a new GaAs waveguide device but also a device interaction length compatible to or even shorter than that of MQW devices

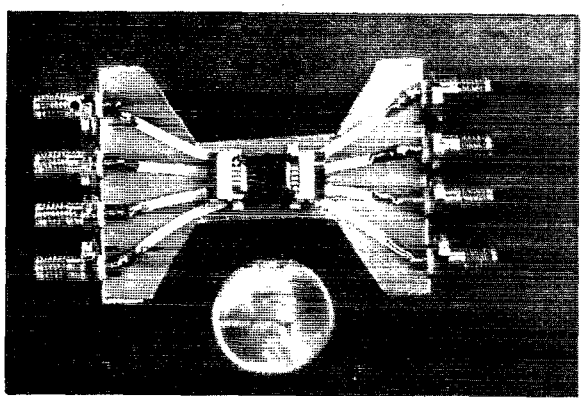

FIG. 4. Fully packaged optically activated modulator (OAM) on a GaAs/GaAlAs rib waveguide.

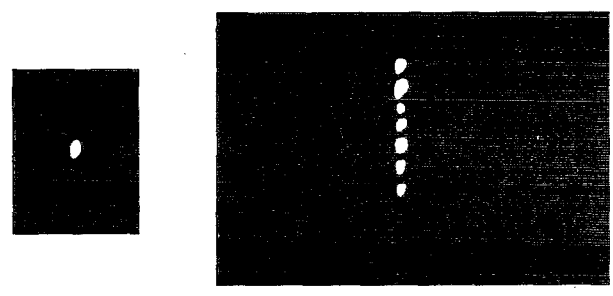

(a) (b)

FIG. 6. Near-field pattern of the single-mode guided wave from a GaAs/GaAlAs channel waveguide. (a) Single-channel and (b) rib waveguide array.

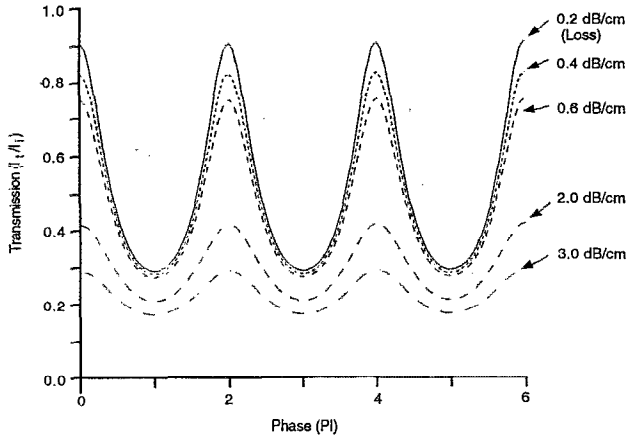

FIG. 7. Transmission (I_t/I_i) of the GaAs OAM as a function of phase shift with the waveguide propagation loss as a parameter.

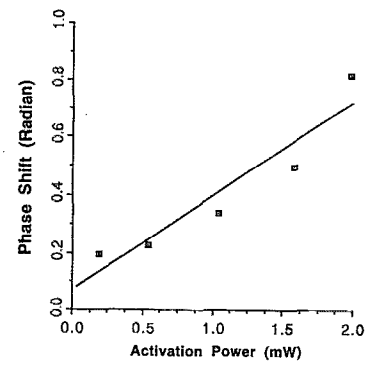

FIG. 9. Photo-induced phase shift in the guided light vs modulating light power with an interaction length of 5 μm.

($\sim$100 μm). For a Fabry–Perot phase modulator, the existence of loss reduces the peak transmission to less than unity. Figure 7 shows the calculated curves of I_t/I_i with different propagation loss as a parameter. The reflectance R is set at 30%, which is also the case at the GaAs/air interface. The amount of phase shift is determined by the Fabry–Perot transmission curves of Fig. 7. It is clear that to increase the device modulation depth, the GaAs/GaAlAs waveguide propagation loss should be reduced to a minimum value. It is obvious that the effective index modulation, i.e., Δn_{eff}, due to optical activation, can be found by measuring the T value. The optically activated modulation is shown in Fig. 8. The top trace is the HeNe 0.633 μm modulating light source and the bottom trace the modulated guided wave (1.3 μm) which was end-fire coupled into the rib waveguide. Modulation depth to 33% was observed for a GaAs waveguide with a 0.4 dB/cm propagation loss. A similar result was also observed by a Mach–Zehnder interferometer.[22] It is clear that in order to increase the throughput intensity, waveguide propagation loss needs to be minimized. Figure 9 shows the measured phase shift as a function of the intensity of the optical activation. To compare the optically activated modulation with a linear electro-optic phase modulator, an ac electrical field was added to the electrode. The experimental results in Fig. 10 conclude that in order to generate the same T value (33% in this case), we need to have a linear electro-optic device with a 1 mm interaction length and 10 V applied voltage. The interaction length is 200 times longer than the linear dimension of the window of the optically activated modulator. Such compactness significantly enhances the packing density of the modulator array. Note that the modulation depth of 33% corresponds to an $\sim$55° phase shift. If the optical window is enlarged to 16.4 μm, i.e., to have π phase shift, the maximum value of T will be generated.

There are three sources of modulation that can be used in the waveguide modulator. They are (1) direct modulation of the 1.3 μm laser diode by varying the current of the laser diode driver; (2) optical activation using the 0.632 μm HeNe laser; and (3) electrical signal applied directly onto the Schottky contact located on top of the rib waveguide (see Fig. 3). Combinations of these modulation mechanisms were tried, and the results are shown in Fig. 11. Note that a combination of these modulation outputs is shown in the bottom trace of the photograph.

C. Waveguide design considerations

The experimental results we observed show that the OAM can work either as a Fabry–Perot phase modulator or a cutoff modulator. Both the phase modulator and the cutoff modulator are single-mode devices that use the same

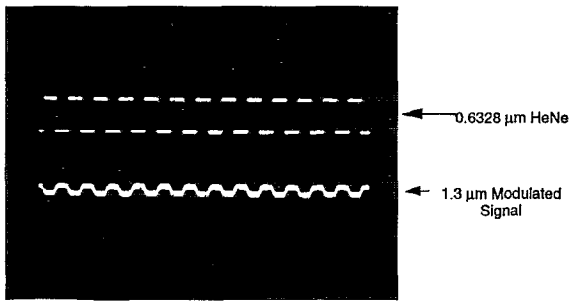

FIG. 8. Optically activated modulator: top trace=0.633 μm modulating light source; bottom trace=modulated 1.3 μm guided wave (modulation speed 4 kHz).

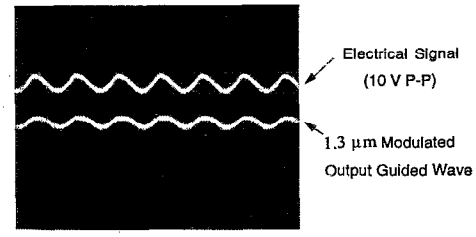

FIG. 10. A 33% modulation depth of the 1.3 μm guided wave throughput generated directly from a 0.5 mm electrode with 10 V peak to peak value at 4 kHz.

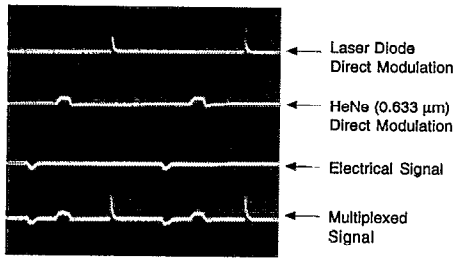

FIG. 11. Detection of the 1.3 μm output signal from the GaAs rib waveguide. Multiplexing of these three signals are shown. The modulation frequency is fixed at 4 kHz.

electrode structure. The difference between them is that the optically activated phase modulator is well above the cutoff condition so that the confinement factor C_f, which is defined as

$$C_f=\frac{|\langle W|W\rangle|_{\text{guiding region}}}{|\langle W|W\rangle|_{\text{guiding region}}+|\langle W|W\rangle|_{\text{cladding regions}}}, \tag{13}$$

is not changed significantly by the existence of an external bias field. In Eq. (13), $|W\rangle$ is the electric field distribution function of the guided mode. In the case of an optically activated modulator working in the cutoff regime, however, the confinement factor, and thus waveguide propagation loss, change drastically due to the existence of an external electric field. The sensitivity of the waveguide confinement factor C_f to the existence of an applied electric field is a major parameter in determining the waveguide's suitability for use as either a phase or a cutoff modulator.

In order to clarify this statement, a theoretical calculation was made to evaluate the influence of the waveguide's effective index on the confinement factor. The experimental results imply that a good optically activated cutoff modulator is achieved by a waveguide with an effective index very close to the substrate index. Therefore, it is essential that the waveguide effective index be in the neighborhood of the cutoff boundary. The small variation of the effective index can be induced by either an external voltage or a small perturbation of waveguide parameters such as aluminum concentration or waveguide dimension.

The rib waveguide used was the subject of calculation. It was found that only the evanescent tail penetrating into the GaAlAs cladding layer was changed significantly. A three-dimensional surface plot with effective index as the x axis, the distance of the waveguide in the depth direction as the y axis (origin at the center of the GaAs guiding layer), and the electric field of the guided mode as the z axis is shown in Fig. 12. The refractive index of $Ga_{0.93}Al_{0.07}As$ is 3.3710 at 1.3 μm. The waveguide depth is varied in the neighborhood of 1 μm. The theoretical calculation shows that, when the effective index is very close to 3.3710, the evanescent tail of the guided wave penetrating into the $Ga_{0.93}Al_{0.07}As$ cladding layer is the major reason for the decrease of the confinement factor. The peak of the electric field clearly decreases as the guided mode index moves

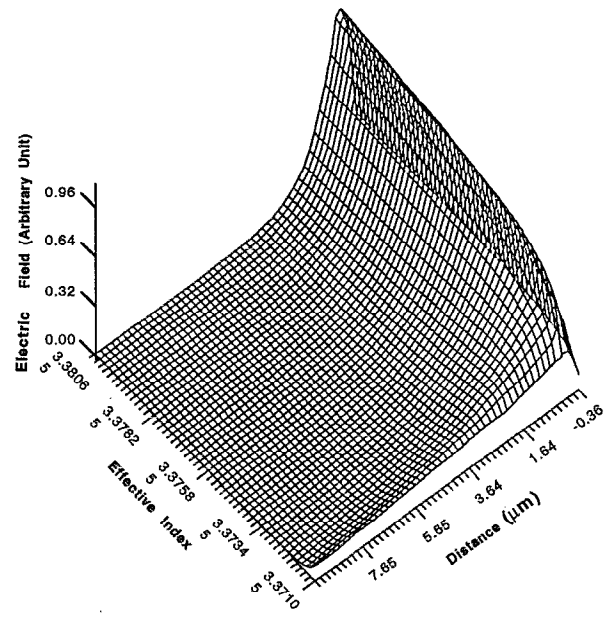

FIG. 12. Propagating mode profiles along the transverse direction of the GaAs waveguide (GaAs-$Ga_{0.93}Al_{0.07}As$). The increase of the evanescent wave is clearly seen.

closer to the cutoff boundary. Each of the waveguide propagating mode profiles shown in Fig. 13 is normalized so that

$$|\langle W|W\rangle|=1, \tag{14}$$

where $|W\rangle$ is the waveguide mode function and the integration covers all of the area. The equal electric field lines of the fundamental mode with various mode indices corresponding to Fig. 12 are shown in Fig. 13. The increase of the intensity of the evanescent tail as the effective index of

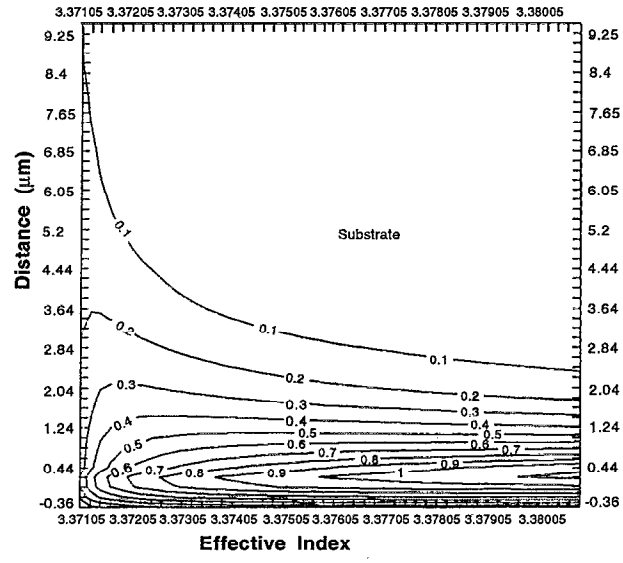

FIG. 13. Equal electrical field topology of the propagating modes of the GaAs waveguide (GaAs-$Ga_{0.93}Al_{0.07}As$) corresponding to Fig. 12.

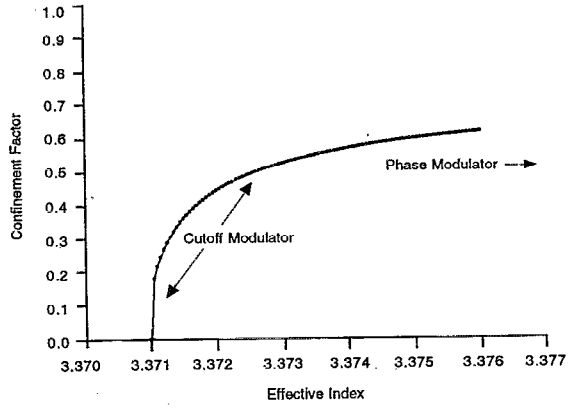

FIG. 14. Confinement factors as a function of effective indices of the GaAs waveguide (GaAs-$Ga_{0.93}Al_{0.07}As$).

the guided mode moves closer to 3.3710 is clearly shown in this figure. The resulting confinement factor, as defined by Eq. (13), is a function of the guided wave mode index and is shown in Fig. 14. The confinement factor drops to zero as N_{eff} shifts to the value of the cladding index. Two regions are evident in Figs. 13 and 14. The first region represents the waveguide domain suitable for a cutoff modulator and where the confinement factor changes drastically as a function of the effective index N_{eff}. The second region is the waveguide domain, suitable for a phase modulator, and where the confinement factor changes slightly under the influence of an external activation source. It is clearly shown in these figures that the dynamic range of the waveguide effective index appropriate for an optically activated phase modulator is larger than that of an optically activated cutoff modulator.

D. Optically activated cutoff modulator

Based on the discussion presented in Sec. III C, a single-mode GaAs-GaAlAs rib waveguide with an effective index closer to the cutoff boundary was tested. The device we tested in this section had a narrower waveguide dimension and was thus closer to the cutoff boundary (Fig. 14). The rest of the setup is the same as that shown in Fig. 5. Operation of the device can be carried out either by shining cw HeNe laser light on the window area and applying the ac signal through the SMA injection port (Fig. 4) or by directly encoding the modulated signal onto the HeNe laser. Figure 15 shows the optically activated modulation by directly modulating the HeNe laser with an electrical chopper. The top trace of the figure is the HeNe laser light and the bottom trace the infrared (IR) throughput from the GaAs rib waveguide. A modulation depth of 8.5 dB was measured. Note that the device was biased at -12 V. The existence of a dc bias voltage significantly enhanced the current effect. Optical activation through current modulation is not polarization-dependent. As a result, both TE and TM modes demonstrated a large magnification of the IR guided wave throughput signal.

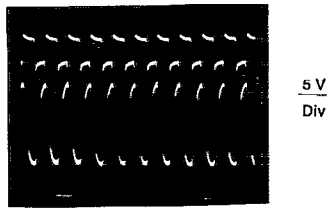

FIG. 15. Optically activated modulation (bottom trace) by pulsing the activation light (top trace). Modulation frequency is 4 kHz.

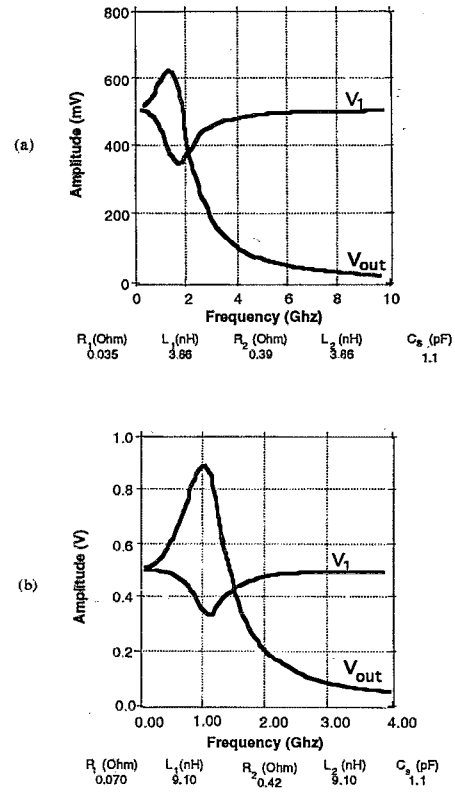

FIG. 16. Computer simulated results of the voltage transfer function of the optoelectronic circuit shown in Fig. 4. V_1 is the voltage at the input SMA connector and V_{out} is the voltage across the rib waveguide.

With respect to the modulation speed of the GaAs/GaAlAs rib waveguide OAM, the first limiting factor is the free-carrier lifetime of the semiconductor material. For undoped GaAs, the carrier lifetime is around 10 ns.[11] Carrier lifetime in the ps and sub-ps range has been achieved in GaAs by using doping or ion implantation techniques.[12,13] As a result of this achievement, the other limiting factor—parasitic RLC factors[25] associated with electronic lumped structures—shall be considered. A computer simulation was made to evaluate the voltage response as a function of the input rf frequency. The results are shown in Fig. 16. Figures 16(a) and 16(b) represent two cases where the maximum and minimum values of the lumped elements for this packaged device are shown.

As far as the lifetime of the optically generated free carriers is concerned, carrier lifetime in the ps to sub-ps range was achieved in GaAs by using doping and ion implantation techniques.[12,13] Accordingly, the modulation speed is not limited by the current effect.

IV. CONCLUSIONS

We presented for the first time, to the best of our knowledge, an optically activated phase modulator (OAM) on a GaAs/GaAlAs heterostructure rib waveguide. Experimental results showed that a device interaction length shorter than that of MQWs is capable of producing an OAM device with a 8.2 dB modulation depth. Theoretical calculations were provided to compare the index modulation between optical activation and the linear electro-optic effect. Experimental work was also conducted to confirm the magnitude of the optically generated index modulation through free-carrier injection. A single-mode GaAs OAM device can be designed either as a phase modulator or as a cutoff modulator. A theoretical calculation based on the variation of the confinement factor as a function of the guided mode effective index was provided. Design criteria for both cases are given. Optically activated modulators using GaAs/GaAlAs rib waveguides were fabricated. Fully packaged devices were demonstrated for both single-channel OAMs and OAM arrays. Optically activated modulation was demonstrated in both phase modulation and cutoff modulation regimes. Signal multiplexing was further conducted using optical activation sources, IR signal carriers, and electrical signals. The modulation speed/bandwidth was also considered and the results showed a multi-Gigahertz device operational bandwidth. Improvement of modulation speed is feasible by employing a traveling wave electrode structure on a semi-insulating substrate. Further applications based on the reported GaAs/GaAlAs rib waveguide devices can be found in Ref. 26.

ACKNOWLEDGMENTS

This research is currently sponsored by AFOSR and SDIO.

[1] M. Papuchon, Appl. Phys. Lett. **27**, 289 (1975).
[2] R. C. Alferness, R. V. Schmidt, and E. H. Turner, Appl. Opt. **18**, 4012 (1979).
[3] W. E. Marin, Appl. Phys. Lett. **32**, 562 (1975).
[4] V. Ramaswamy, M. D. Divino, and R. D. Standley, Appl. Phys. Lett. **32**, 644 (1978).
[5] C. L. Chang and C. S. Tsai, Appl. Phys. Lett. **43**, 22 (1983).
[6] S. Y. Wang, S. H. Lin, and M. Huong, Appl. Phys. Lett. **51**, 83 (1987).
[7] R. T. Chen, Appl. Phys. Lett. **54**, 2628 (1989).
[8] R. T. Chen and C. S. Tsai, Opt. Lett. **11**, 546 (1986).
[9] J. C. Campbell, F. A. Blum, D. W. Shaw, and K. L. Lawley, Appl. Phys. Lett. **27**, 202 (1975).
[10] R. T. Chen and C. S. Tsai, IEEE J. Quantum Electron. **QE-23**, 2205 (1987).
[11] S. M. Sze, *Physics of Semiconductor Devices*, 2nd ed. (Wiley, New York, 1981), p. 851.
[12] See, for example, D. H. Auston, Appl. Phys. Lett. **26**, 101 (1975); J. A. Buck, K. K. Li, and J. R. Whinnery, J. Appl. Phys. **51**, 769 (1980); P. Cheung, IEEE Trans. Microwave Theory Technol. **38**, 586 (1990); and C. H. Lee, IEEE Trans. Microwave Theory Technol. **38**, 596 (1990).
[13] M. B. Johnson and T. C. McGill, Appl. Phys. Lett. **54**, 2424 (1989).
[14] R. A. Soref and B. R. Bennett, IEEE J. Quantum Electron. **QE-23**, 123 (1987).
[15] J. P. Lorenzo and R. A. Soref, Appl. Phys. Lett. **51**, 6 (1987).
[16] J. Manning, R. Olshansky, and C. B. Su, Electron. Lett. **21**, 496 (1985).
[17] N. K. Dutta, N. A. Olsson, and W. T. Tsang, Appl. Phys. Lett. **45**, 836 (1984).
[18] K. Tada and Y. Okada, IEEE Electron Device Lett. **EDL-7**, 605 (1986).
[19] O. Mikami and H. Nakagome, Electron. Lett. **20**, 228 (1984).
[20] K. Ishida, H. Nakamura, R. Matsumura, T. Kadoi, and H. Inoue, Appl. Phys. Lett. **50**, 141 (1987).
[21] N. W. Ashcroft, *Solid State Physics* (Cornell University, Ithaca, NY, 1976).
[22] Z. Y. Cheng and C. S. Tsai, Appl. Phys. Lett. **59**, 18, 2222 (1991).
[23] B. G. Streetman, *Solid State Electronic Devices* (Prentice-Hall, Englewood Cliffs, NJ, 1980).
[24] Purchased from Epitronics, AZ.
[25] "Lead Inductance Comparisons," Semiconductor Int. 74 (June 1988).
[26] R. T. Chen, "An Optically Activated Modulator on GaAs/GaAlAs Compound Semiconductor Channel Waveguide," Final Report to AFOSR, Contract No. F49620-90-C-0068 (1991).